01 Aug 2017

Realizing Structural Color Generation with Aluminum Plasmonic V-Groove Metasurfaces

W. Wang

D. Rosenmann

D. Czaplewski

Xiaodong Yang
Missouri University of Science and Technology, yangxia@mst.edu

et. al. For a complete list of authors, see https://scholarsmine.mst.edu/mec_aereng_facwork/3734

Recommended Citation

W. Wang et al., "Realizing Structural Color Generation with Aluminum Plasmonic V-Groove Metasurfaces," *Optics Express*, vol. 25, no. 17, pp. 20454-20465, Optical Society of America, Aug 2017.
The definitive version is available at https://doi.org/10.1364/OE.25.020454

Realizing structural color generation with aluminum plasmonic V-groove metasurfaces

WEI WANG,[1] DANIEL ROSENMANN,[2] DAVID A. CZAPLEWSKI,[2] XIAODONG YANG,[1,3] AND JIE GAO[1,*]

[1]*Department of Mechanical and Aerospace Engineering, Missouri University of Science and Technology, Rolla, MO 65409, USA*
[2]*Center for Nanoscale Materials, Argonne National Laboratory, Argonne, IL 60439, USA*
[3]*yangxia@mst.edu*
[*]*gaojie@mst.edu*

Abstract: Structural color printing based on all-aluminum plasmonic V-groove metasurfaces is demonstrated under both bright field and dark field illumination conditions. A broad visible color range is realized with the plasmonic V-groove arrays etched on an aluminum surface by simply varying the groove depth while keeping the groove period as a constant. Polarization dependent structural color printing is further achieved with interlaced V-groove arrays along both the horizontal and vertical directions. These results pave the way towards the use of an all-aluminum structural color printing platform for many practical applications such as security marking and information storage.

OCIS codes: (050.6624) Subwavelength structures; (240.6680) Surface plasmons; (160.3918) Metamaterials; (330.1690) Color.

References and links

1. C. Genet and T. W. Ebbesen, "Light in tiny holes," Nature **445**(7123), 39–46 (2007).
2. Q. Chen and D. R. S. Cumming, "High transmission and low color cross-talk plasmonic color filters using triangular-lattice hole arrays in aluminum films," Opt. Express **18**(13), 14056–14062 (2010).
3. D. Inoue, A. Miura, T. Nomura, H. Fujikawa, K. Sato, N. Ikeda, D. Tsuya, Y. Sugimoto, and Y. Koide, "Polarization independent visible color filter comprising an aluminum film with surface-plasmon enhanced transmission through a subwavelength array of holes," Appl. Phys. Lett. **98**(9), 093113 (2011).
4. Z. Li, W. Wang, D. Rosenmann, D. A. Czaplewski, X. Yang, and J. Gao, "All-metal structural color printing based on aluminum plasmonic metasurfaces," Opt. Express **24**(18), 20472–20480 (2016).
5. S. J. Tan, L. Zhang, D. Zhu, X. M. Goh, Y. M. Wang, K. Kumar, C. W. Qiu, and J. K. W. Yang, "Plasmonic color palettes for photorealistic printing with aluminum nanostructures," Nano Lett. **14**(7), 4023–4029 (2014).
6. A. S. Roberts, A. Pors, O. Albrektsen, and S. I. Bozhevolnyi, "Subwavelength plasmonic color printing protected for ambient use," Nano Lett. **14**(2), 783–787 (2014).
7. J. S. Clausen, E. Højlund-Nielsen, A. B. Christiansen, S. Yazdi, M. Grajower, H. Taha, U. Levy, A. Kristensen, and N. A. Mortensen, "Plasmonic metasurfaces for coloration of plastic consumer products," Nano Lett. **14**(8), 4499–4504 (2014).
8. S. Choudhury, U. Guler, A. Shaltout, V. M. Shalaev, A. V. Kildishev, and A. Boltasseva, "Pancharatnam–Berry phase manipulating metasurface for visible color hologram based on low loss silver thin film," Adv. Opt. Mater. **5**(10), 1700196 (2017).
9. X. Li, L. Chen, Y. Li, X. Zhang, M. Pu, Z. Zhao, X. Ma, Y. Wang, M. Hong, and X. Luo, "Multicolor 3D meta-holography by broadband plasmonic modulation," Sci. Adv. **2**(11), e1601102 (2016).
10. W. Wan, J. Gao, and X. Yang, "Full-color plasmonic metasurface holograms," ACS Nano **10**(12), 10671–10680 (2016).
11. Y.-W. Huang, W. T. Chen, W.-Y. Tsai, P. C. Wu, C.-M. Wang, G. Sun, and D. P. Tsai, "Aluminum plasmonic multicolor meta-hologram," Nano Lett. **15**(5), 3122–3127 (2015).
12. H. J. Park, T. Xu, J. Y. Lee, A. Ledbetter, and L. J. Guo, "Photonic color filters integrated with organic solar cells for energy harvesting," ACS Nano **5**(9), 7055–7060 (2011).
13. B. Zeng, Y. Gao, and F. J. Bartoli, "Ultrathin nanostructured metals for highly transmissive plasmonic subtractive color filters," Sci. Rep. **3**(1), 2840 (2013).
14. M. J. Uddin, T. Khaleque, and R. Magnusson, "Guided-mode resonant polarization-controlled tunable color filters," Opt. Express **22**(10), 12307–12315 (2014).
15. S. Yokogawa, S. P. Burgos, and H. A. Atwater, "Plasmonic color filters for CMOS image sensor applications," Nano Lett. **12**(8), 4349–4354 (2012).

#292733 https://doi.org/10.1364/OE.25.020453
Journal © 2017 Received 13 Apr 2017; revised 21 Jun 2017; accepted 30 Jun 2017; published 14 Aug 2017

16. Z. Li, A. W. Clark, and J. M. Cooper, "Dual color plasmonic pixels create a polarization controlled nano color palette," ACS Nano **10**(1), 492–498 (2016).
17. G. Si, Y. Zhao, J. Lv, M. Lu, F. Wang, H. Liu, N. Xiang, T. J. Huang, A. J. Danner, J. Teng, and Y. J. Liu, "Reflective plasmonic color filters based on lithographically patterned silver nanorod arrays," Nanoscale **5**(14), 6243–6248 (2013).
18. T. Ellenbogen, K. Seo, and K. B. Crozier, "Chromatic plasmonic polarizers for active visible color filtering and polarimetry," Nano Lett. **12**(2), 1026–1031 (2012).
19. J. Do, M. Fedoruk, F. Jäckel, and J. Feldmann, "Two-color laser printing of individual gold nanorods," Nano Lett. **13**(9), 4164–4168 (2013).
20. C. Saeidi and D. van der Weide, "Bandwidth-tunable optical spatial filters with nanoparticle arrays," Opt. Express **22**(10), 12499–12504 (2014).
21. T. Xu, Y. K. Wu, X. Luo, and L. J. Guo, "Plasmonic nanoresonators for high-resolution colour filtering and spectral imaging," Nat. Commun. **1**(5), 59 (2010).
22. A. F. Kaplan, T. Xu, and L. J. Guo, "High efficiency resonance-based spectrum filters with tunable transmission bandwidth fabricated using nanoimprint lithography," Appl. Phys. Lett. **99**(14), 143111 (2011).
23. F. Cheng, J. Gao, T. S. Luk, and X. Yang, "Structural color printing based on plasmonic metasurfaces of perfect light absorption," Sci. Rep. **5**(1), 11045 (2015).
24. F. Cheng, J. Gao, L. Stan, D. Rosenmann, D. Czaplewski, and X. Yang, "Aluminum plasmonic metamaterials for structural color printing," Opt. Express **23**(11), 14552–14560 (2015).
25. F. Cheng, X. Yang, D. Rosenmann, L. Stan, D. Czaplewski, and J. Gao, "Enhanced structural color generation in aluminum metamaterials coated with a thin polymer layer," Opt. Express **23**(19), 25329–25339 (2015).
26. K. Kumar, H. Duan, R. S. Hegde, S. C. W. Koh, J. N. Wei, and J. K. W. Yang, "Printing colour at the optical diffraction limit," Nat. Nanotechnol. **7**(9), 557–561 (2012).
27. X. M. Goh, Y. Zheng, S. J. Tan, L. Zhang, K. Kumar, C. W. Qiu, and J. K. W. Yang, "Three-dimensional plasmonic stereoscopic prints in full colour," Nat. Commun. **5**, 5361 (2014).
28. Y. C. Liang, W. Wang, J. S. Moon, and J. G. Winiarz, "Enhancement in the photorefractive performance of organic composites photosensitized with functionalized CdSe quantum dots," Opt. Mater. **58**, 203–209 (2016).
29. N. Fang, H. Lee, C. Sun, and X. Zhang, "Sub-diffraction-limited optical imaging with a silver superlens," Science **308**(5721), 534–537 (2005).
30. L. Sun, X. D. Yang, W. Wang, and J. Gao, "Diffraction-free optical beam propagation with near-zero phase variation in extremely anisotropic metamaterials," J. Opt. **17**(3), 035101 (2015).
31. N. Liu, T. Weiss, M. Mesch, L. Langguth, U. Eigenthaler, M. Hirscher, C. Sönnichsen, and H. Giessen, "Planar metamaterial analogue of electromagnetically induced transparency for plasmonic sensing," Nano Lett. **10**(4), 1103–1107 (2010).
32. R. Adato, A. A. Yanik, J. J. Amsden, D. L. Kaplan, F. G. Omenetto, M. K. Hong, S. Erramilli, and H. Altug, "Ultra-sensitive vibrational spectroscopy of protein monolayers with plasmonic nanoantenna arrays," Proc. Natl. Acad. Sci. U.S.A. **106**(46), 19227–19232 (2009).
33. H. Wei, Z. Wang, X. Tian, M. Käll, and H. Xu, "Cascaded logic gates in nanophotonic plasmon networks," Nat. Commun. **2**, 387 (2011).
34. Y. K. R. Wu, A. E. Hollowell, C. Zhang, and L. J. Guo, "Angle-insensitive structural colours based on metallic nanocavities and coloured pixels beyond the diffraction limit," Sci. Rep. **3**(1), 1194 (2013).
35. T. Xu, H. Shi, Y. K. Wu, A. F. Kaplan, J. G. Ok, and L. J. Guo, "Structural colors: from plasmonic to carbon nanostructures," Small **7**(22), 3128–3136 (2011).
36. M. A. Kats, R. Blanchard, P. Genevet, and F. Capasso, "Nanometre optical coatings based on strong interference effects in highly absorbing media," Nat. Mater. **12**(1), 20–24 (2013).
37. K. Chung, S. Yu, C. J. Heo, J. W. Shim, S. M. Yang, M. G. Han, H. S. Lee, Y. Jin, S. Y. Lee, N. Park, and J. H. Shin, "Flexible, angle-independent, structural color reflectors inspired by morpho butterfly wings," Adv. Mater. **24**(18), 2375–2379 (2012).
38. T. W. Ebbesen, H. J. Lezec, H. F. Ghaemi, T. Thio, and P. A. Wolff, "Extraordinary optical transmission through sub-wavelength hole arrays," Nature **391**(6668), 667–669 (1998).
39. H. S. Lee, Y. T. Yoon, S. S. Lee, S. H. Kim, and K. D. Lee, "Color filter based on a subwavelength patterned metal grating," Opt. Express **15**(23), 15457–15463 (2007).
40. H. Park, Y. Dan, K. Seo, Y. J. Yu, P. K. Duane, M. Wober, and K. B. Crozier, "Filter-free image sensor pixels comprising silicon nanowires with selective color absorption," Nano Lett. **14**(4), 1804–1809 (2014).
41. K. Seo, M. Wober, P. Steinvurzel, E. Schonbrun, Y. Dan, T. Ellenbogen, and K. B. Crozier, "Multicolored vertical silicon nanowires," Nano Lett. **11**(4), 1851–1856 (2011).
42. C. L. Haynes, A. D. McFarland, L. L. Zhao, R. P. Van Duyne, G. C. Schatz, L. Gunnarsson, J. Prikulis, B. Kasemo, and M. Kall, "Nanoparticle optics: The importance of radiative dipole coupling in two-dimensional nanoparticle arrays," J. Phys. Chem. B **107**(30), 7337–7342 (2003).
43. J. A. Schuller, E. S. Barnard, W. Cai, Y. C. Jun, J. S. White, and M. L. Brongersma, "Plasmonics for extreme light concentration and manipulation," Nat. Mater. **9**(3), 193–204 (2010).
44. H. A. Atwater and A. Polman, "Plasmonics for improved photovoltaic devices," Nat. Mater. **9**(3), 205–213 (2010).
45. H. X. Deng, T. C. Wang, J. Gao, and X. D. Yang, "Metamaterial thermal emitters based on nanowire cavities for high-efficiency thermophotovoltaics," J. Opt. **16**(3), 035102 (2014).

46. G. V. Naik, V. M. Shalaev, and A. Boltasseva, "Alternative plasmonic materials: beyond gold and silver," Adv. Mater. **25**(24), 3264–3294 (2013).
47. J. Zhang, J. Y. Ou, N. Papasimakis, Y. Chen, K. F. Macdonald, and N. I. Zheludev, "Continuous metal plasmonic frequency selective surfaces," Opt. Express **19**(23), 23279–23285 (2011).
48. V. R. Shrestha, S. S. Lee, E. S. Kim, and D. Y. Choi, "Aluminum plasmonics based highly transmissive polarization-independent subtractive color filters exploiting a nanopatch array," Nano Lett. **14**(11), 6672–6678 (2014).
49. V. Kulkarni, E. Prodan, and P. Nordlander, "Quantum plasmonics: optical properties of a nanomatryushka," Nano Lett. **13**(12), 5873–5879 (2013).
50. T. Søndergaard, S. M. Novikov, T. Holmgaard, R. L. Eriksen, J. Beermann, Z. Han, K. Pedersen, and S. I. Bozhevolnyi, "Plasmonic black gold by adiabatic nanofocusing and absorption of light in ultra-sharp convex grooves," Nat. Commun. **3**, 969 (2012).
51. http://www.inplainviewwinnipeg.com/prairie_stained_glass.shtml, https://www.prairiestudioglass.com/

1. Introduction

Recently, various types of structural color printing techniques have been introduced to generate a wide range of visible colors with great potential to replace the traditional pigment-based color printing technology [1–4]. Among these techniques, plasmonic metamaterials and metasurfaces are becoming more attractive for structural color applications due to their advanced light manipulation capabilities [5–7]. Plasmonic metasurfaces are also widely used to realize ultrathin color holograms for reconstructing complex holographic images [8–11]. Different kinds of plasmonic nanostructures have been employed to generate high resolution structural colors, including one-dimensional gratings [12–14], hole arrays [1–3, 15, 16], antenna arrays [7, 17–20], metal-insulator-metal structures [6, 21–25], and combined nanodisk and nanohole arrays [5, 26, 27]. Optical resonances across the whole visible spectrum can be achieved by adjusting the geometrical parameters of the plasmonic nanostructures, according to the tunable spectral responses of propagating surface plasmons (SP) [4, 28–32], localized surface plasmon resonances (LSPR) [4, 21, 33–38], and Fabry-Pérot cavity modes [4, 39]. Plasmonic color generation has been utilized in obtaining highly saturated color with narrow spectral width [4, 6, 40, 41], color filtering with extraordinary optical transmission [4, 12–14], high-resolution color imaging [4, 21, 39,42], color filtering with polarization dependence [4, 32, 33, 43–45], and angle-insensitive structural colors [4, 39, 45]. Nobel metals such as silver [13, 23, 26, 34] and gold [6] are widely used in previous plasmonic color printing works due to their lower ohmic losses in the visible spectrum. However, silver is not ideal for color generation because it is susceptible to oxidation and sulphidation [5, 17, 46] and gold has limitations for rendering blue colors due to the interband transition [4, 6, 47, 48]. Alternatively, aluminum has been used as an attractive plasmonic material for structural color generation due to its excellent optical response over the entire visible spectrum, chemical and thermal stability due to its self-limiting impermeable native oxidation layer, low cost, and complementary metal oxide semiconductor (CMOS) compatibility [7, 15, 16, 24, 25, 48, 49]. Although many aluminum based metasurfaces with plasmonic structures such as metal-insulator-metal structures [6, 13, 14, 22–25] or combined nanodisk and nanohole arrays [5, 26, 27] have been proposed for color printing, the complex fabrication process will not only increase the production cost but also degrade the color performance.

Here we propose and demonstrate structural color printing with high color performance based on plasmonic V-groove metasurfaces of an aluminum surface, by using a simple but efficient one-step focused ion beam milling process. A wide visible color range can be realized under both bright field and dark field illumination conditions by only varying the groove depth while maintaining a constant groove period. The optical mode analysis in aluminum V-groove arrays reveals the excitation of electric dipole and magnetic dipole resonances for the structural color generation. The incident angle dependent optical reflection and scattering from the V-groove metasurface color printing platform is also studied. Furthermore, polarization dependent structural color printing under both bright field and dark field illumination conditions is demonstrated with interlaced V-groove arrays along both the

horizontal and vertical directions. The demonstrated all-aluminum structural color printing based on plasmonic V-groove metasurfaces provides great opportunities for many color related applications such as security marking, information storage, and microscale imaging.

2. Metasurface fabrication and characterization

A typical one-dimensional V-shaped groove array on an aluminum surface designed as gap surface plasmon nanostructures for structural color printing is schematically illustrated in Fig. 1(a). By adjusting the groove depth *d*, while keeping the groove period *p* as a constant, the plasmonic resonance frequency of the V-groove etched on the aluminum film with thickness *h* can be tuned across the whole visible spectrum and thus a wide visible color range can be realized. The designed aluminum plasmonic metasurfaces for color printing are fabricated as follows. A 250 nm aluminum film is deposited on a silicon wafer using a Lesker PVD250 electron-beam evaporator at a rate of 12 Å/sec. The designed V-groove arrays are then directly milled on the aluminum surface by a focused ion beam (FIB) milling process (FEI Helios Nanolab 600 DualBeam) with a gallium ion current of 9.7 pA and an accelerating voltage of 30 KeV. The groove period *p* is selected as 250 nm and the groove depth *d* is increased from 76 nm to 231 nm for the fabricated groove structures. Figures 1(c)-1(j) are the cross-section SEM images of the fabricated V-groove arrays with eight groove depths from 76 nm to 231 nm at a tilted view angle of 52 degrees. During the FIB process, straight line patterns with designed width of 10 nm are milled on the aluminum surface. By controlling the ion beam exposure time, V-grooves with various depths are directly formed. The measured side wall angle of the V-groove is around 73 degrees. As shown in Figs. 1(c) and 1(d), when the groove depth is small, the bottom tip of the fabricated V-groove is not very sharp, but this geometrical imperfection will not affect the color performance since the groove depth is the major controlling parameter for the plasmonic spectral resonance.

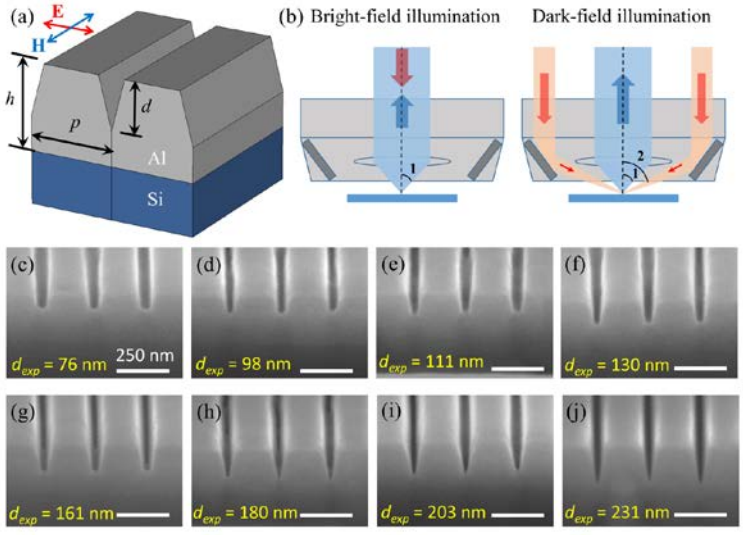

Fig. 1. (a) Schematic of the V-groove array on an aluminum layer with silicon substrate. (b) Schematic of the optical reflection mode for the bright field and dark field illumination. Angle 1 represents the collection angle of the objective lens while angle 2 is the incident angle of the dark field condenser lens. (c-j) Cross-section SEM images of the fabricated V-groove arrays with the same groove period of 250 nm and eight different groove depths from 76 nm to 231 nm. Scale bars: 250 nm.

The optical reflection and scattering response from the fabricated V-groove arrays are measured under both bright field and dark field illumination conditions. Figure 1(b) is the

schematic of a typical optical reflection mode for the bright field and dark field illumination through a 20x microscope objective lens with NA = 0.4 (Nikon BD Plan). Under bright field illumination condition, the incident light is focused through the central lens and the reflected light from the metasurface is collected by the same optical path at a half Angle 1 of 23.6 degrees. Under dark field illumination condition, the incident light is focused onto the metasurface through the annular condenser lens at an incident Angle 2 around 70 degrees, and the back-scattered light from the sample is collected by the central lens in a confocal setup. Due to the limited penetration depth in the thick aluminum film for incident light in the visible range, optical transmission from the V-groove metasurfaces will be effectively blocked. With the *p*-polarized light (where the electric field is perpendicular to the groove direction), a gap surface plasmon mode localized inside the V-groove will be excited. Depending on the groove depth, plasmonic modes at various resonance wavelengths will be realized across the visible range to provide different reflective colors.

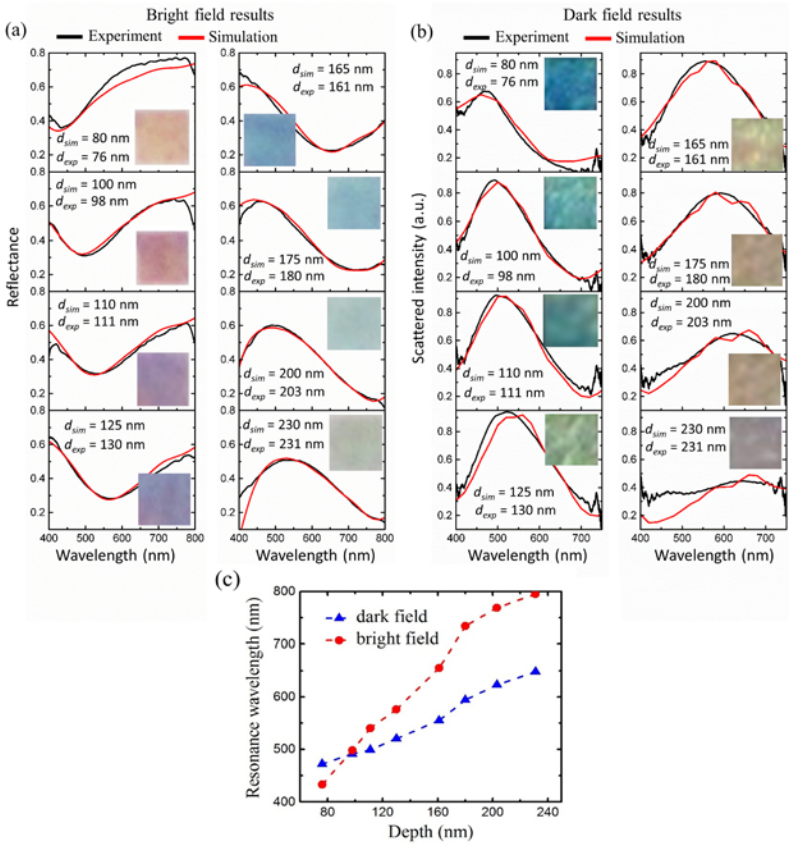

Fig. 2. (a) Measured (black solid line) and simulated (red solid line) optical reflectance spectra under bright field illumination for the eight V-groove arrays with different measured groove depths from 76 nm to 231 nm, while the depths used in the simulation from 80 nm to 230 nm are also listed. (b) Measured (black solid line) and simulated (red solid line) scattering intensity spectra under dark field illumination for the eight V-groove arrays. Insets show the corresponding bright field or dark field optical microscope images of 20 × 20 μm^2 V-groove arrays. (c) Dependence of the red-shift of the plasmonic resonance dip under bright field illumination (red) and the plasmonic resonance peak under dark field illumination (blue) on the groove depth.

The optical reflectance and scattering intensity spectra from the fabricated V-groove arrays under bright field and dark field illumination are obtained within the visible

wavelength range from 400 nm to 800 nm with a halogen lamp and an optical spectrometer (LR1, ASEQ instruments). Each fabricated V-groove metasurface has an area of 20×20 μm^2 in the measurements. Figure 2 summarizes the measured optical reflection spectra under bright field illumination and the optical scattering intensity spectra under dark field illumination, as well as the corresponding microscope images shown in the insets, for the eight V-groove arrays shown in Figs. 1(c)-1(j) with different groove depths from 76 nm to 231 nm. The bright field reflectance spectra as shown in Fig. 2(a) exhibit a red-shifted plasmonic resonance dip changing from 433 nm to 795 nm. The reflective colors also change from yellow, magenta to cyan as the groove depth is increased, which are the primary colors of CMYK system. The simulation results calculated from finite-difference time-domain (FDTD) method are also plotted. In the bright field reflection simulation, a plane wave impinges vertically on the metasurface and the permittivities of aluminum (imaginary part multiplied by factor of 3 to account for fabrication-induced losses) and silicon substrate are obtained from the refractive index database [46]. In Fig. 2(b), the dark field scattering intensity spectra from the same set of V-groove arrays are presented. The spectral resonance peak varies from 474 nm to 656 nm as the groove depth is increased. The scattering colors also change from blue, green to orange, which cover the primary colors of the RGB system. It is noted that for the V-groove arrays with the depth of 230 nm, the resonance peak is shifted above 600 nm. However, the resonance peak is very broad with low scattering intensity so that grayish color is obtained. It is noted that light can penetrate through the aluminum film as the groove depth is close to the film thickness and get dissipated in the silicon substrate. Therefore, as the groove depth is further increased, the scattering intensity contrast becomes smaller and the scattering spectrum gets broader. Another effect is that more optical energy in a wider wavelength range is absorbed due to the adiabatic nanofocusing [50]. By increasing the Al film thickness, the optical energy penetrated into the silicon substrate can be decreased to enhance the scattered density. In order to further improve the color contrast and color performance of the device, different plasmonic materials with low optical absorption loss such as silver can be used to obtain much narrower plasmonic resonances. However, there is one issue that silver surface is not stable in ambient environment and the sample surface should be protected by an additional polymer or dielectric layer from oxidation and sulphidation. The dependence of the red-shift of the plasmonic resonance dip under bright field illumination and the plasmonic resonance peak under dark field illumination on the groove depth is shown in Fig. 2(c). It shows that the plasmonic resonances of the V-groove structures follow nearly linear relations with the groove depths. The wavelength variation range of the plasmonic resonance under bright field illumination is almost twice of that under dark field illumination, showing a wider color response range for the bright field illumination compared to the dark field illumination. These results are very useful to guide the color painting generation in Section 3. In the dark field scattering simulation, the metasurface is illuminated by a plane wave with an oblique incident angle of 70 degrees. The back scattered light in the simulation is collected over a conical solid angle corresponding to the numerical aperture of the 20x microscope objective lens used in the experiment. The far field scattering intensity is calculated and integrated within the half angle of 23.6 degrees as illustrated in Fig. 1(b). A good match between the experimental and simulation results for both the bright field and dark field results are found in Fig. 2. The measured reflection spectra and scattering intensity spectra depicted in Fig. 2 are further converted as the discrete points in the CIE 1931 xy chromaticity coordinates based on color theory in Fig. 3, illustrating the color gamut of the fabricated V-groove metasurfaces. Figure 3(b) shows the zoomed in data area in Fig. 3(a), together with the simulation results. It is shown that the chromaticity coordinates for the bright field reflection results evolve in a clockwise fashion while the dark field scattering results vary in a counterclockwise way, as the groove depth is increased. All the coordinates are around the achromatic point, demonstrating a large degree of the color range tuning for the designed V-groove metasurfaces.

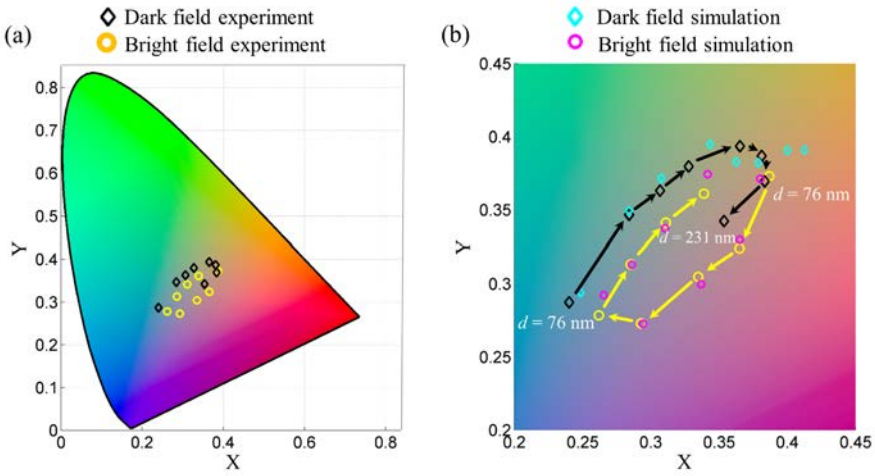

Fig. 3. Measured and simulated results in the CIE 1931 xy chromaticity coordinates for the eight V-groove arrays with the increased groove depth from 76 nm to 231 nm. The circles and diamonds represent the bright field and dark field results, respectively.

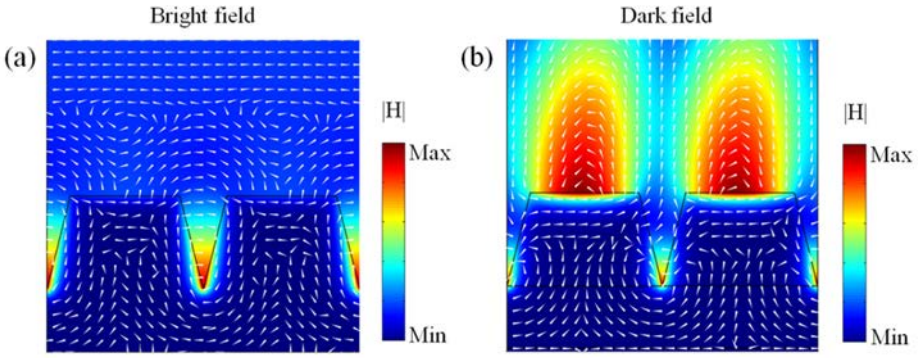

Fig. 4. Cross sections of the time-averaged magnetic field (color map) and electric displacement (white arrows) distributions for the V-groove metasurface with depth of 150 nm at the resonance wavelength, under (a) the bright field illumination with vertical incident angle and (b) the dark field illumination with oblique incident angle of 70 degrees.

For the purpose of understanding the physical mechanism of the gap surface plasmon modes localized inside the V-groove nanostructure, time-averaged magnetic field (color map) and electric displacement (white arrows) distributions for the V-groove with depth of 150 nm at the resonance wavelength are plotted in Fig. 4 under both the bright field and dark field illumination. As shown in Fig. 4(a) under the bright field illumination with vertical incident light, strong magnetic dipole resonance inside the V-groove is observed with the concentrated magnetic field surrounded by an electric displacement flow loop. At the same time, an electric dipole resonance is also excited on the top surface of the aluminum ridge. The excitation of the gap surface plasmon mode within the aluminum V-groove provides strong optical absorption for the vertical incident light at the resonance wavelength so that the subtractive color can be observed in the bright field reflection spectrum from the metasurface. Figure 4(b) plots the optical mode distributions for the V-groove under the dark field illumination with oblique incident angle of 70 degrees. The magnetic dipole resonance confined inside the groove gets very week, while a strong magnetic dipole resonance occurs around the top aluminum-air interface of the aluminum ridge, together with the electric dipole resonance at the top aluminum surface. It is observed that the electromagnetic energy is scattered away

from the V-groove into the far field above the groove at the resonance wavelength. Therefore, the additive color can be obtained in the dark field scattering spectrum above the metasurface. The above mode analysis indicates that different structural colors will be realized under the bright field as well as under dark field illumination conditions.

The incident angle dependent optical spectral response is further studied in simulation for the V-groove metasurface with depth of 100 nm, under both the bright field and dark field illumination conditions. For the calculated optical reflection spectra under bright field illumination as shown in Fig. 5(a), when the incident angle changes from 0 degree (vertical direction) to around 50 degrees, the reflection resonance dip almost remains at the same wavelength, giving unchanged color for different view angles. When the incident angle is larger than 50 degrees, the gap surface plasmon mode supported inside the V-groove disappears and the metasurface behaves like a broadband mirror. For the optical scattering intensity spectra under the dark field illumination as plotted in Fig. 5(b), the scattering resonance peak almost linearly red-shifts to longer wavelength when the incident angle increases, and the resonance peak width and scattering intensity also depend on the incident angle. It is shown that the scattering intensity will reach its maximum value at the incident angle of 84 degrees.

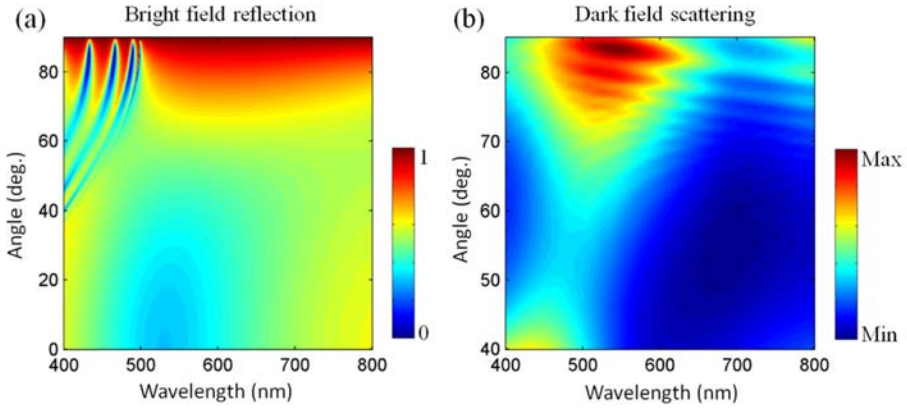

Fig. 5. (a) Simulated incident angle dependent (a) optical reflection spectra under the bright field illumination and (b) optical scattering intensity spectra under the dark field illumination for the V-groove metasurface with depth of 100 nm.

When two-dimensional V-groove sample with different groove depths along two orthogonal directions is considered, each set of V-groove array along either horizontal or vertical direction can be excited by a certain linear polarization so that the sample can show different color responses. The simulation schematic for one two-dimensional V-groove sample is shown in Fig. 6(a) with the groove side wall angle of 73 degrees, and the groove depths along two orthogonal directions are d_1 = 155 nm and d_2 = 100 nm, respectively. Figure 6(b) plots the reflectance spectrum for each groove array excited by either horizontal or vertical linear polarization. The horizontal linear polarization excites the plasmonic resonance of the groove array with depth d_1, while the vertical linear polarization excites the plasmonic resonance of the groove array with depth d_2. It shows that the reflectance spectrum from the sample can be controlled by the incident linear polarization so that different color responses will be achieved.

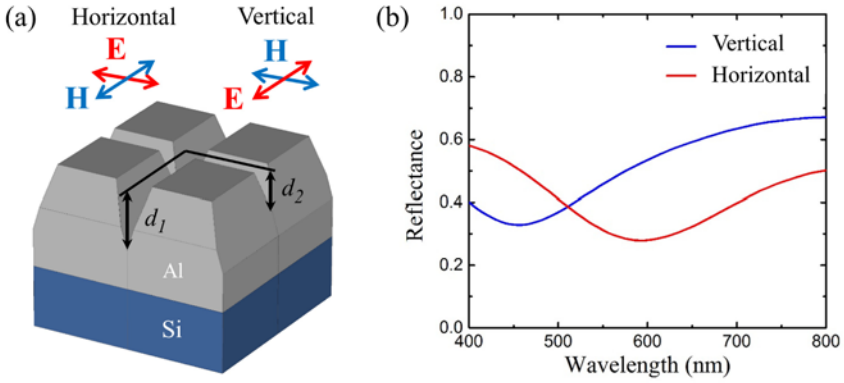

Fig. 6. (a) Schematic of two-dimensional V-groove array on an aluminum layer with silicon substrate. The grooves in horizontal and vertical directions have different depths, giving different color responses depending on the incident linear polarizations. (b) Simulated reflectance spectra of the sample illuminated by light with either horizontal or vertical linear polarization. Different polarization illumination will result in different color responses.

3. Plasmonic painting of color images

In order to demonstrate the applicability and visual performance of the proposed aluminum plasmonic V-groove metasurfaces for structural color printing applications, a micrometer scale 40 × 50 μm^2 plasmonic printed copy of a landscape art painting drawn by ourselves, which is modified from a stained glass design by Prairie Studio Glass (Winnipeg, MB, Canada) [51], as displayed in Fig. 7(a), is fabricated. By choosing the V-groove array with certain groove depth in each pixel, the desired colors can be realized with high fidelity and visual contrast. The measured bright field microscope image of the plasmonic painting under the horizontal linear polarization (white arrow, 0 degree) as shown in Fig. 7(b) successfully reproduces the original image features and colors shown in Fig. 7(a). Figure 7(c) illustrates the measured dark field microscope image, where nearly complementary colors are displayed as expected. The SEM images of the fabricated plasmonic painting sample with vertical V-groove arrays are shown in Figs. 7(d)-7(f). When the vertical linear polarization (90 degrees) is used to excite the V-grooves, the color will disappear which can be used in security applications. Figure 8(a) shows the color responses of the measured bright field microscope images for the one-dimensional V-groove painting sample with different linear polarization angles. In the bright field setting, the linear polarizer was placed in the incident beam path. It is shown that the reflection color will disappear when the polarization is parallel to the V-grooves (90 degrees). Figure 8(b) shows the color responses of the measured dark field microscope images with different linear polarization angles. In the dark field setting, the oblique incident beam polarization cannot be controlled easily, so the linear polarizer is placed in the vertical scattering beam path. The results show that the scattering beam from the V-grooves is also highly polarized even when the incident beam is unpolarized because only *p*-polarized wave can be scattered. The scattering color will disappear when the polarization is parallel to the V-grooves (90 degrees). It is noteworthy that the color responses of the sample with unpolarized light are almost the same as the cases with 45-degree polarization angle, because the unpolarized light can be decomposed into two orthogonal linear polarizations.

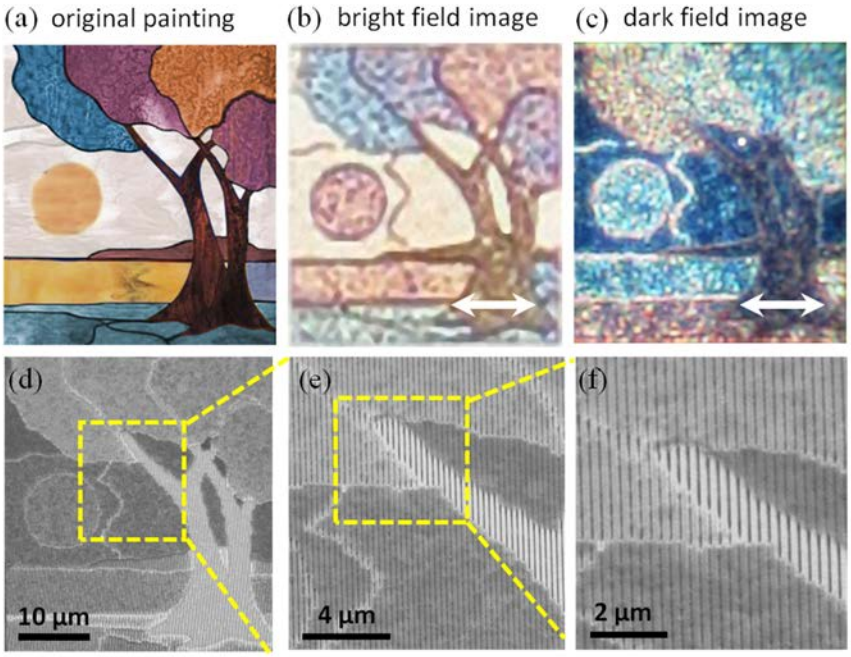

Fig. 7. (a) Original landscape art painting with various colors drawn by ourselves. (b) The measured bright field microscope image of the plasmonic painting under the horizontal linear polarization (white arrow) with size of 40 × 50 μm^2. (c) The measured dark field microscope image. (d)-(f) SEM images of the fabricated plasmonic painting sample with V-groove arrays of different depths. SEM image in panel (f) is tilted at a view angle of 52 degrees.

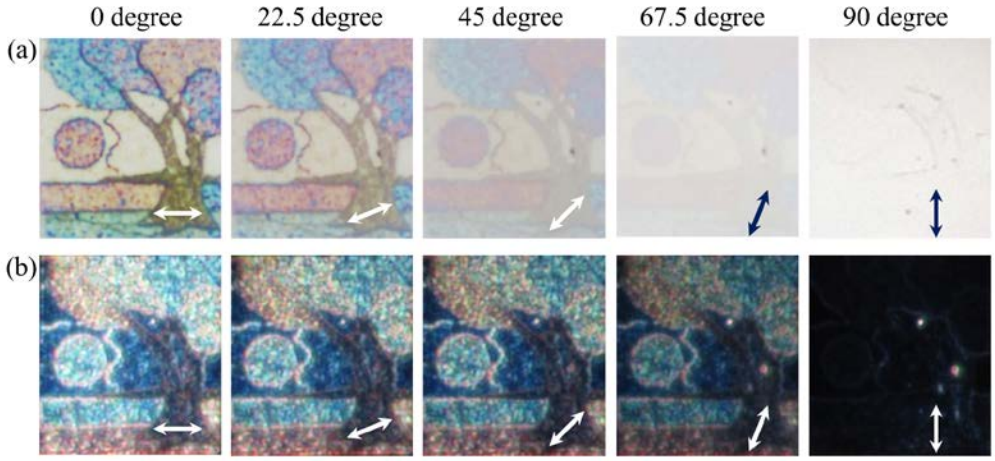

Fig. 8. (a) Color responses of the measured bright field microscope images for the one-dimensional V-groove painting sample with different linear polarization angles from 0 degree to 90 degrees. The linear polarizer is placed in the incident beam path. (b) Color responses of the measured dark field microscope images for the one-dimensional V-groove painting sample with different linear polarization angles. The linear polarizer is placed in the vertical scattering beam path. The scattering beam from the sample is highly polarized.

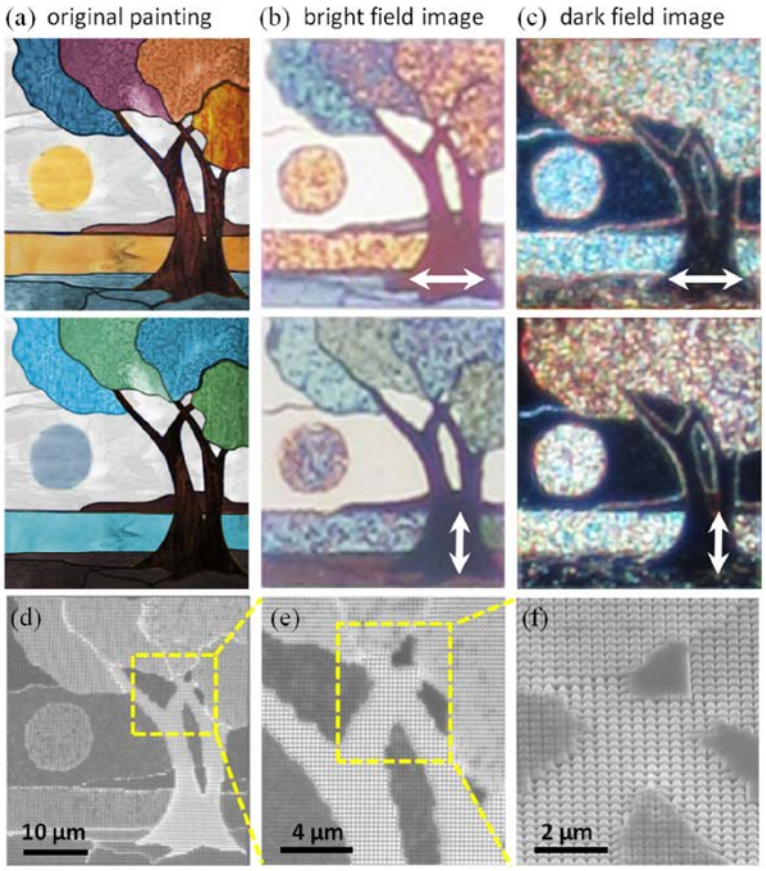

Fig. 9. (a) Original landscape art paintings with two different color sets drawn by ourselves. (b) The measured bright field microscope images of the plasmonic painting under the horizontal and vertical linear polarizations (white arrows). (c) The measured dark field microscope images. (d)-(f) SEM images of the fabricated plasmonic painting sample with the interlaced vertical and horizontal V-groove arrays. SEM image in panel (f) is tilted at a view angle of 52 degrees to clearly show the V-groove arrays along both directions.

Since the current one-dimensional V-groove array works under a certain linear polarization perpendicular to the groove direction, two-dimensional V-groove arrays along both the horizontal and vertical directions can be interlaced together for displaying images with polarization-dependent colors. Two original landscape art paintings with different color sets drawn by ourselves are displayed in Fig. 9(a), where the top one is designed to use vertical V-groove arrays under the horizontal linear polarization while the bottom one is for horizontal V-groove arrays under the vertical linear polarization. Figure 9(b) gives the measured bright field microscope images under two different linear polarizations, showing the vivid image colors switching from one set to another once the linear polarization is tuned from horizontal to vertical (white arrows). The measured dark field microscope images are also switched under orthogonal linear polarization excitation. The SEM images of the fabricated plasmonic painting sample with the interlaced vertical and horizontal V-groove arrays are shown in Figs. 9(d)-9(f). Figure 10(a) shows the color responses of the measured bright field microscope images for the two-dimensional V-groove painting sample with different linear polarization angles. When the linear polarizer is rotated, the color images will gradually change from one color set to the other color set as expected. While the two color sets are mixed at the 45-degree polarization angle. Figure 10(b) shows the color responses of the measured dark field microscope images with different linear polarization angles, where

the scattering colors also vary gradually between the two color sets. This feature of polarization-dependent color response is important for applications of security marking and information storage. The demonstrated plasmonic painting results indicate that the proposed all-aluminum structural color printing platform based on the V-groove metasurfaces is capable of creating high-resolution color images with high brightness and saturation.

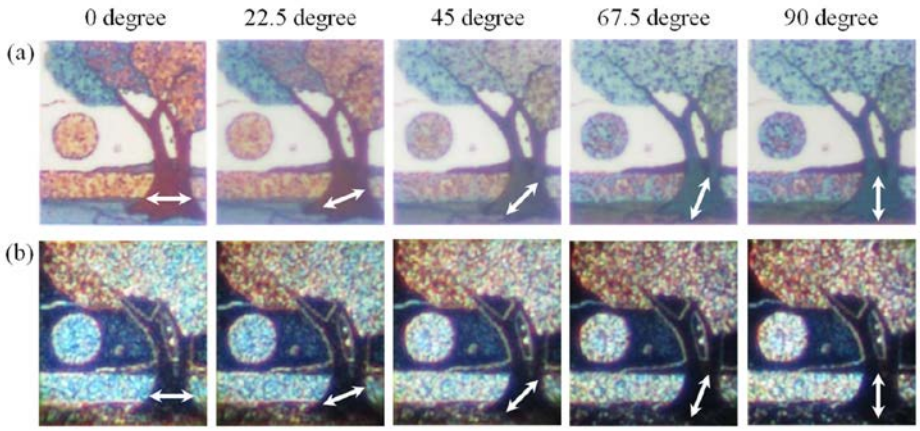

Fig. 10. (a) Color responses of the measured bright field microscope images for the two-dimensional V-groove painting sample with different linear polarization angles from 0 degree to 90 degrees. The linear polarizer is placed in the incident beam path. (b) Color responses of the measured dark field microscope images for the two-dimensional V-groove painting sample with different linear polarization angles. The linear polarizer is placed in the vertical scattering beam path.

4. Conclusion

An all-aluminum structural color printing platform based on plasmonic V-groove metasurfaces with high resolution and high color performance have been introduced and demonstrated, by using a one-step focused ion beam milling process. By only adjusting the groove depth, the plasmonic resonances of the V-groove arrays can be tuned across the whole visible spectrum, resulting in either the subtractive colors obtained from the reflection spectra under the bright field illumination, or the complimentary additive colors resulting from the scattering spectra under the dark field illumination. The reproduced polarization dependent plasmonic paintings of color images under both the bright field and dark field illumination conditions manifest the feasibility and flexibility of all-aluminum plasmonic V-groove metasurfaces for structural color printing applications. The demonstrated aluminum plasmonic V-groove metasurfaces for high-performance and pigment-free structural color generation will open many new possibilities for realizing relevant applications such as security marking, information storage, and microscale imaging.

Funding

National Science Foundation (NSF) (ECCS-1653032, DMR-1552871, CBET-1402743); Office of Naval Research (ONR) (N00014-16-1-2408); U.S. Department of Energy (DE-AC02-06CH11357)

Acknowledgment

The authors thank Zhigang Li for the useful discussion and acknowledge the facility support from the Materials Research Center at Missouri S&T. This work was performed, in part, at the Center for Nanoscale Materials, a U.S. Department of Energy, Office of Science, Office of Basic Energy Sciences User Facility under Contract No. DE-AC02-06CH11357.